# Topochemical polymerization in microparticles of crystalline triazine-based monomers: Study by conventional and ultra-fast chip calorimetry

Evgenii V Komov, Alexey P Melnikov, Alexey A Piryazev, Alina V Maryasevskaya, Artyom O Petrov, Georgiy V Malkov, Alexey V Shastin, Denis V Anokhin, Dimitri A Ivanov

# Topochemical polymerization in microparticles of crystalline triazine-based monomers: study by conventional and ultra-fast chip calorimetry

Evgenii V. Komov,[⊥] Alexey P. Melnikov,[⊥,‡] Alexey A. Piryazev,[⊥,‡] Alina V. Maryasevskaya,[⊥,‡] Artyom O. Petrov, [‡] Georgiy V. Malkov,[‡] Alexey V. Shastin, [‡] Denis V. Anokhin,[⊥, ‡] and Dimitri A. Ivanov [*, ⊥, ‡, ‖]

[⊥]Lomonosov Moscow State University (MSU), 1 Leninskie Gory, 119991 Moscow, Russia

[‡]Federal Research Center of Problems of Chemical Physics and Medicinal Chemistry of RAS, Academician Semenov av. 1, 142432 Chernogolovka, Russia

[‖]Institut de Sciences de Matériaux de Mulhouse-IS2M, CNRS UMR 7361, Jean Starcky, 15, F-68057 Mulhouse, France

*Corresponding author: Dimitri A. Ivanov, Email: dimitri.ivanov@uha.fr

**Abstract**: The work addresses complex thermal behavior of two triazine-based azide-alkyne monomers: 2-azido-4,6-bis(prop-2-yn-1-yloxy)-1,3,5-triazine (ABPOT) and 2,4-diazido-6-(prop-2-yn-1-yloxy)-1,3,5-triazine (DAPOT). Despite the similarity of the two $AB_2$-type structures, the isothermal aging kinetics of DAPOT occurs significantly faster than that of ABPOT. During storage at room temperature, the chemical transformation starts in the crystalline state via topochemical reactions. Calorimetry, along with X-ray diffraction, makes it possible to probe transformations in isolated microcrystals including melting, oligomerization, polymerization and decomposition. The thermal behavior of microparticles can strongly differ from that of the same material in bulk due to enhanced contribution of the monomer evaporation at the particle surface at extremely high heating rates. The isothermal melting caused by the topochemical reaction and subsequent polymerization during long-term storage can be modeled using the correlated two-stage Avrami equation. The Avrami parameter corresponding to the amorphization process is close to unity while that of the polymerization is approximately 0.5. Consequently, both processes can likely be viewed as one-dimensional, with diffusion control dominating the polymerization process. The observed impact of long-term storage on the polymerization capability of the monomers may prove beneficial in synthesizing hyperbranched polymers through "green" topochemical methods.

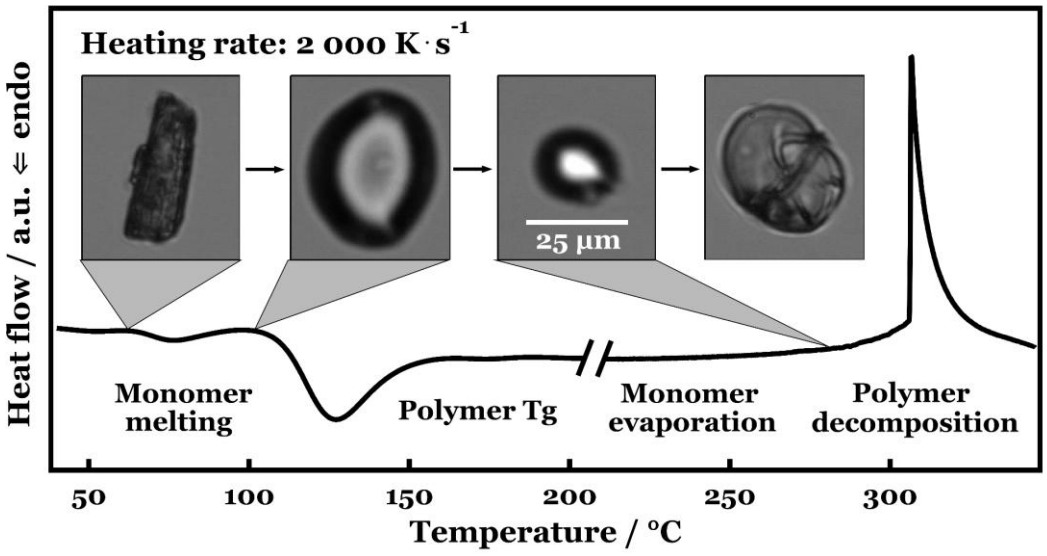


**Table of Contents**

**Keywords:** triazines, azide-alkyne cycloaddition, click chemistry, topochemical reaction, solid-state polymerization, microparticles, fast scanning calorimetry, X-ray diffraction

## 1. Introduction

Over the last two decades, much attention has been paid to the development of «click» chemistry routes such as Diels-Alder and thiol-ene reactions. This approach constitutes an easy, efficient, and environmentally friendly way to obtain the desired compounds. However, the complexity of tracking multiple parameters responsible for the structure and properties of the target polymers limits the use of these methods for industrial production [1].

Since the «green» methods employ transformations under moderate conditions, spontaneous solid-state reactions at temperatures much lower than the melting points of the initial compounds represent a significant problem. Topochemical processes and, in particular, solid-state polymerization (SSP) have been extensively investigated in the past [2]. It was found that SSP of monomers with conjugated triple bonds can represent a universal way to synthesize crystalline polymers with high molecular weight and fully conjugated main chains [3,4]. In this case, the monomer melting enthalpy is usually higher than the enthalpy of polymerization [5-8], which explains the fact that the process can proceed in the solid phase. There are also some reports showing transformation of a reaction blend to a lower ordered or even amorphous state due to localized melting of monomers caused by the exothermic effect of polymerization [5-7,9,10].

One of the most common solid-state reactions is a topochemical azide-alkyne cycloaddition (TAAC) involving two neighboring molecules located in appropriate conformation in crystal lattice with 1,4- or 1,5-disubstituted 1,2,3-triazole products [11]. The underlying principle in topochemical reactions is the proper arrangement of reactants to control the stereochemistry of the product without disordering. Several reports describe synthesis of biomolecules by preliminarily arranging the azide and alkyne groups at specific positions such that the non-covalent interactions (e.g., hydrogen bonding, arene-perfluoroarene interactions, etc.) pertinent to other submolecular fragments would help assembling the molecules in a favorable way for the following chemical reactions [11-13]. The difference in the distances between azide and alkyne groups to give 1,4- and 1,5-regioisomers was identified as one of the decisive factors that influenced the regioselectivity [14]. It is also known that the solid-state reactions of numerous investigated molecules show preferred regioselectivity for 1,4-triazole products [13].

An important difference between TAAC and other topochemical reactions lies in the nature of the initiator. While most of the known topochemical reactions require light for activation [7,10], TAAC represents a thermally activated reaction. Depending on the activation barrier, the reactions can happen spontaneously at room temperature or at elevated temperatures [6,11]. It was also demonstrated that the activation energy of thermally-induced SSP could be many times higher than for photopolymerization [12]. For practical applications it is important to control the activation energy and manage the thermally induced AAC processes in the solid phase [15].

The present work is focused on thermal behavior of two $AB_2$-type crystalline monomers: 2-azido-4,6-bis(prop-2-yn-1-yloxy)-1,3,5-triazine (ABPOT) and 2,4-diazido-6-(prop-2-yn-1-yloxy)-1,3,5-triazine (DAPOT) (cf. Scheme 1) [16]. Both monomers are employed in the form of individual microparticles and in bulk. The initial stages of topochemical polymerization of crystalline azide-alkyne monomers are addressed with the help of conventional differential scanning calorimetry (DSC) and nanocalorimetry. The latter technique, which is also known as fast scanning calorimetry (FSC) on a chip, allows performing thermal measurements at high heating and cooling rates, i.e. up to $10^5$ K $s^{-1}$ [17,18]. Such conditions make it possible to kinetically bypass the processes of chemical transformation of the monomers during heating in order to characterize the thermal behavior of the sample without inducing its uncontrolled modification during the heating ramp. More importantly, FSC can be combined with other methods of *in situ* analysis such as FTIR or Raman spectroscopy to better understand the mechanisms of structural evolution in the course of different thermal treatments. Recently, FSC was used in combination with optical microscopy and micro- and nanofocus X-ray diffraction to tackle the structure and thermal properties of gold glyconanoparticles [19], linear [20,21], semicrystalline [22-26] and thermoplastic [27] polymers. It was also used for studies of glassy organic films [28]. The effectiveness of this relatively

recent method in the analysis of individual particles of energetic materials during fast heating has also been demonstrated in the past [29].

## 2. Materials and Methods

The studied triazine-based compounds are soluble in polar organic solvents such as DMSO and DMF; they have a high enthalpy of formation and contain mutually reactive azide and alkyne end groups that allow synthesizing new energetic materials [30]. The reactions of 1,3-dipolar cycloaddition (1,3-DCA) of azides to unsaturated alkynes are applicable for the synthesis of nitrogen-containing energetic and bioactive materials with good selectivity and high yield [16]. They can also be used to obtain hyperbranched polymers (cf. Scheme S1) [1,30] in solutions, the kinetics of which was also specifically addressed [31].

To avoid spontaneous chemical transformation all synthesized samples were stored in sealed containers in a refrigerator at -25 °C.

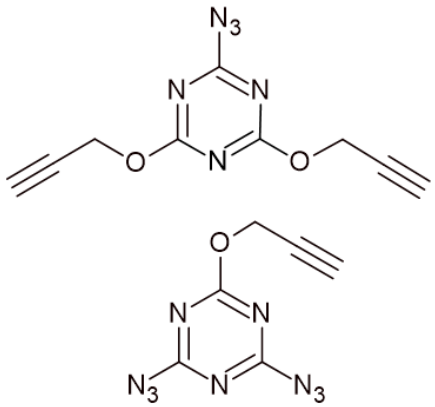

**Scheme 1.** Structure formulas of the ABPOT (top) and DAPOT (bottom) monomers.

Preliminary characterization of the newly synthesized monomers was carried out using conventional methods of physical and chemical analysis. Fig. S1 presents TGA curves measured on fresh DAPOT and ABPOT monomers. The initial weight loss at 170 °C corresponds to the first stage of thermal decomposition, where, according to the mass-spectral analysis of the gaseous products, almost pure nitrogen (93 wt%) is released. This fact, as well as the data of FTIR analysis, indicate an almost complete conversion of azide groups and triazole rings. Further thermal behavior can be explained by isomerization of propargyloxy-triazine fragments, cross-linking of triple bonds, etc. [1,16,31]. To avoid dehydration at 100 °C, which can be caused by high polarity and hygroscopicity of the compounds, the samples needed to be stored in a drying chamber before experiments.

Differential scanning calorimetry (DSC) measurements were performed using DSC 214 Polyma (Netzsch GmbH, Germany) in a nitrogen atmosphere. Monomer samples with a mass between 1 and 10 mg were heated at a rate of 10 K $min^{-1}$.

Thermogravimetric analysis (TGA) experiments were carried out using TGA Q50 (TA Instruments, USA) in a nitrogen atmosphere. Samples with mass ranging from 1 to 3 mg were placed in an open platinum crucible and heated at a rate of 10 K $min^{-1}$ from 25 to 900 °C.

The FSC experiments were carried out with the custom-made equipment, described in our previous work [26]. The samples were placed on XEN-39392 nanocalorimetric sensors (Xensor Integration, Netherlands) with an active area of 100 × 100 $\mu m^2$. Three reference materials were used for temperature calibration of nanocalorimetric sensors: ultra-pure indium, zinc and tin powder (Alfa Aesar, USA). The masses of the particles were estimated from the values of specific melting enthalpy obtained by DSC.

Optical microscopy experiments were carried out on Axio Scope A1 (Carl Zeiss AG, Germany) polarizing optical microscope with a LTS420 heating stage (Linkam scientific instruments ltd., UK) and a digital CMOS camera. For *in situ* FSC experiments, digital high-speed camera Phantom Miro C110 (Vision Research Inc., USA) was coupled to the microscope using a standard C-mount camera adapter. A rising-edge analog signal generated by the FSC controller was used to trigger the camera with a time

delay of less than 2 μs. This setup allows to capture 16-bit grayscale images with a resolution of 1280 × 720 pixels at a frequency of 1 frame/K during controllable heating/cooling ramps at rates up to 1000 K $s^{-1}$.

For wide-angle X-ray scattering (WAXS) experiments a laboratory diffractometer with two-dimensional LX170-HS (Rayonix, USA) detector was used. The norm of the scattering vector **s** ($|s| = 2 \sin\Theta / \lambda$) was calibrated using silver behenate powder diffraction at constant wavelength $\lambda$ of 1.5418 Å.

## 3. Results and discussion

Fig. 1 (A, C) displays DSC heating curves of DAPOT and ABPOT monomers including freshly synthesized samples, as well as the ones measured after storage at room temperature at 25 °C and in the fridge at -25 °C. In choosing the temperature range of DSC measurements we used the TGA data for both pristine monomers (Fig. S1) that were recorded at the same heating rate of 10 K $min^{-1}$. The latter suggests that the thermal decomposition of azide groups and triazole rings proceeds at about 170 °C, which prompted us to limit the DSC temperature range to approx. 165 °C.

The DSC curves of fresh monomers demonstrate endothermic melting peaks with specific enthalpy values of ca. 105 J $g^{-1}$ (cf. 92-105 J $g^{-1}$ in [31]) for both studied monomers and with onset values of 57 (cf. 57-58 °C in [16]) and 41 °C (cf. 40-41 °C in [1]) for DAPOT and ABPOT, respectively. With the increase of storage time the enthalpy of fusion decays, which can be correlated to the loss of initial crystal fraction in the sample. Apart from the melting event, the DSC curves show an intense exothermic polymerization peak in the molten state starting at around 80 °C with specific enthalpy values of ca. 1050 J $g^{-1}$, which nicely compares with the literature value of 1000-1150 J $g^{-1}$ [31]. Importantly, in the course of storage the enthalpy decrease of the exothermic peak is paralleled to a decrease of the enthalpy of fusion. Therefore, both trends reflect a progressively growing amorphous fraction in the sample.

As far as the X-ray diffraction data is concerned (Fig. 1 (B, D)), both as-prepared monomers exhibit sharp diffraction peaks that confirm their highly crystalline initial state. During storage at RT for more than one month or at -25 °C for a few years, the intensity of DAPOT crystalline peaks almost completely vanishes. In contrast, the ABPOT sample demonstrates a much higher stability: during the experimental timeframe its crystallinity remains almost invariant at both storage temperatures used in the study.

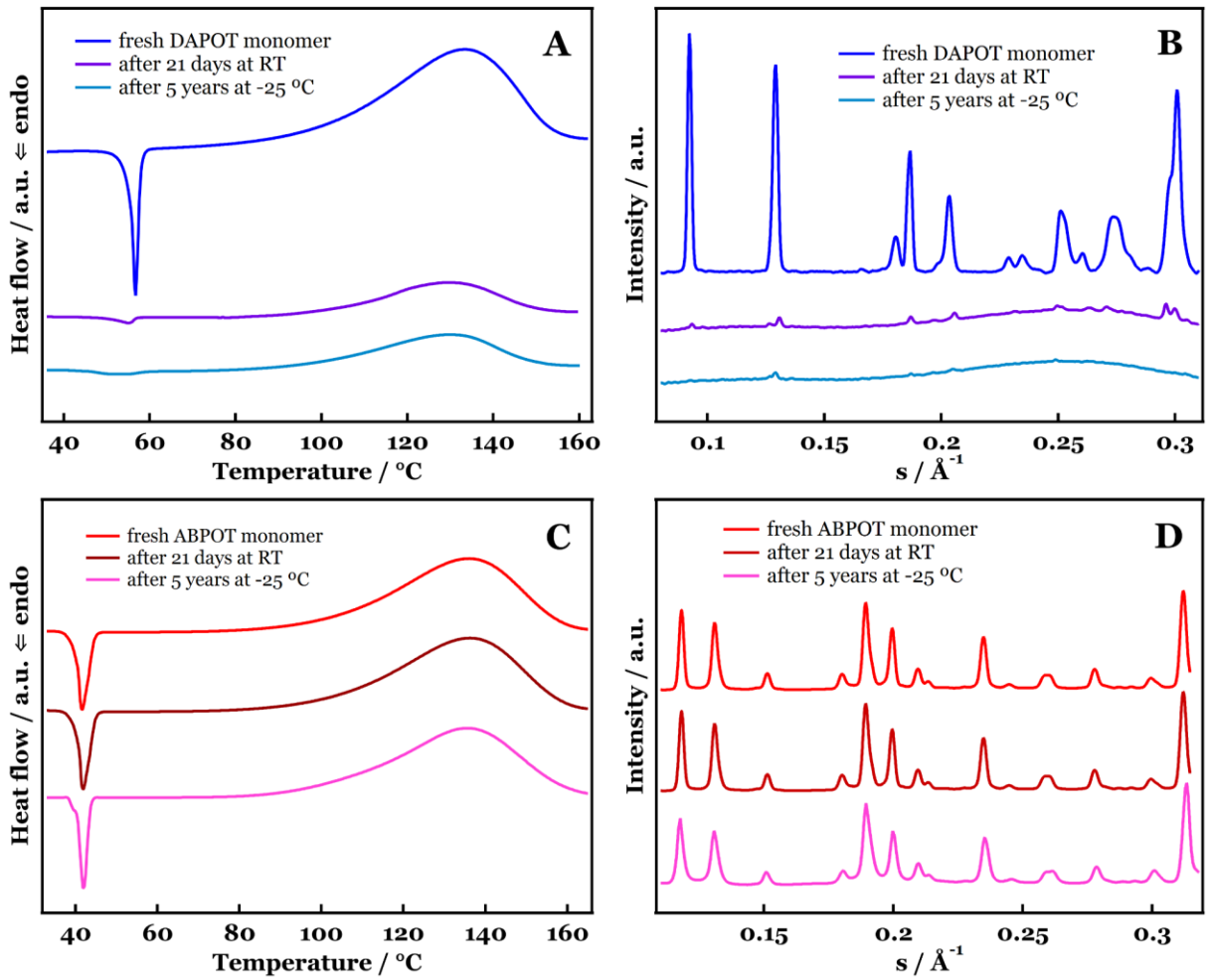


**Fig. 1.** Top row: DSC heating curves (A) and one-dimensional diffraction patterns (B) of DAPOT obtained for initial monomer (blue) and after long-term storage at RT (purple) and at -25 °C (light-blue). Bottom row: DSC curves (C) and one-dimensional diffraction patterns (D) of ABPOT obtained for initial monomer (red), after long-term storage at RT (brown) and at -25 °C (pink). The curves are shifted vertically for clarity.

Amorphization of a crystalline DAPOT monomer at temperatures significantly below its melting point can occur by direct SSP or by a two-step process of local isotropization followed by oligomerization in the isotropic state. The results of a detailed study of the kinetics of the aging process of DAPOT obtained by WAXS and DSC methods are presented in figures 2 and 3, respectively. From the X-ray powder patterns it can be seen that crystallinity of DAPOT gradually decreases to ca. 15 % during the first two weeks of annealing at RT, with a slower transition to a completely amorphous state occurring in the following 23 days (Fig. 2). Regarding the DSC data, it is also observed that the evolution of the melting peak is characterized not only by a decrease in enthalpy but also by a slight decrease in the onset temperature (Fig. 3), which points to a more defect crystal structure of the forming monomer-oligomer blend.

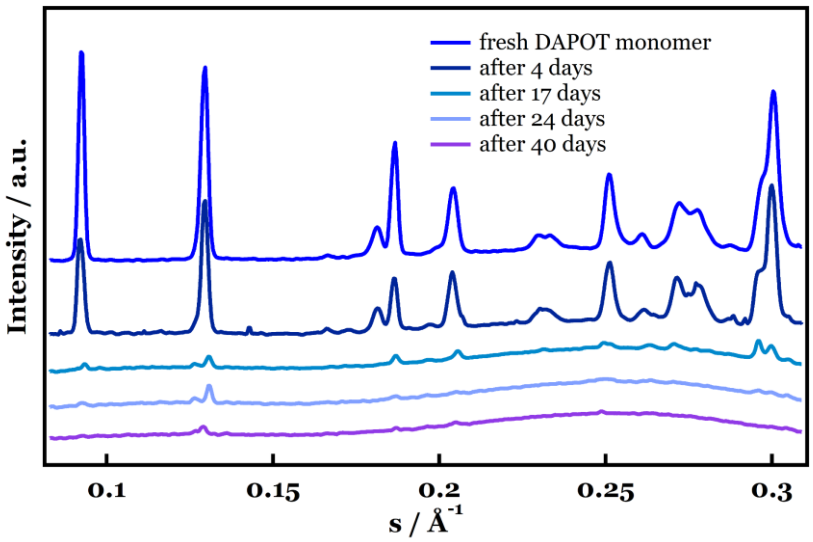


**Fig. 2**. WAXS powder patterns obtained on a DAPOT sample during long-term storage at room temperature. The curves are shifted vertically for clarity.

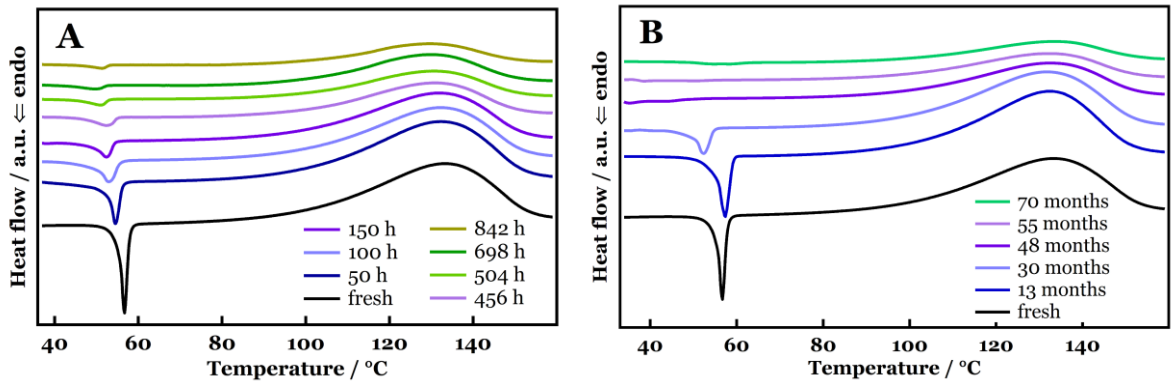


**Fig. 3**. DSC heating curves (10 K min$^{-1}$) of DAPOT samples stored at RT (A) and at -25 °C (B). The curves are shifted vertically for clarity.

To better understand the mechanisms of the processes occurring in the samples during storage we will separately follow the conversions of the amorphization $\alpha_{am}$ and polymerization stages $\alpha_{pol}$. We define the conversions as follows:

$$\alpha_{am}(t) = 1 - \frac{\Delta H_m(t)}{\Delta H_m(0)},\ \alpha_{pol}(t) = 1 - \frac{\Delta H_{pol}(t)}{\Delta H_{pol}(0)}, \qquad (1)$$

where $\Delta H_m(t)$ and $\Delta H_{pol}(t)$ denote the enthalpies of the melting and polymerization processes at time t. Both conversions are obtained by normalization of the corresponding enthalpies to time t=0, which corresponds to the freshly synthesized highly crystalline samples. The functions $\alpha_{am}(t)$ and $\alpha_{pol}(t)$ relevant to storage of DAPOT at RT and at -25 °C were calculated according to Eq. (1) and plotted via dots in Fig. 4 (A, B), respectively. The graph shows that the amorphization occurs noticeably faster than the polymerization. Therefore, it is logical to assume that the process starts with a topochemical reaction in the crystalline state that causes local melting of the crystal. The polymerization leading to a purely amorphous polymer material then proceeds in the molten state. Consequently, it is expected that the correlated two-step model of crystal-to-polymer transition is more relevant for the description of the process. The primary amorphization stage due to the topochemical process is assumed to follow the Avrami kinetics:

$$\alpha_{am}(t) = 1 - exp(-K_1(t - t_0)^{n_1}\ ), \qquad (2)$$

where K, n and $t_0$ are the rate constant, Avrami parameter and the amorphization induction time, respectively.

The kinetics of the second, i.e. the polymerization stage, is supposed to be linked to the first one. In this case, as soon as the amorphization occurs in an elementary volume of the sample at time θ according to Eq. (2) the polymerization process starts. Such a two-stage process can be described with the correlated parallel double-Avrami equation as follows:

$$\alpha_{pol}(t) = \int_{t_0}^{t} \alpha_{pol}(t-\theta) \times \frac{d}{d\theta}\left(\alpha_{am}(\theta)\right) d\theta,$$

$$\alpha_{pol}(t) = K_1 n_1 \int_{t_0}^{t} [1 - exp(-K_2(t-\theta)^{n_2}] \times (\theta - t_0)^{n_1-1} exp(-K_1(\theta - t_0)^{n_1}) d\theta, \qquad (3)$$

where $n_1$, $K_1$, $n_2$, $K_2$ are the Avrami parameters and the rate constants of the first and second processes, respectively. This approach is similar to a modified Hillier-type model that was originally used to incorporate two-stage crystallization processes into the classical Avrami equation [32-34].

It is curious that since the introduction of the model in 1964 in the paper by Gordon and Hillier [35] in the form similar to Eq. (3) there has been quite some confusion in the literature concerning the exact equation describing such a process. Indeed, in his follow-up paper from 1965 Hillier inverted the two processes in the equation [32]. Later, some typos in the equations describing the double-stage process in the paper by Hsiao [36] were remarked in ref. [33]. However, the authors of [33] made a mistake themselves inverting the first and second process in their equation (2). In our work, we keep the initial meaning of the double correlated Avrami process where the incremental conversion of the first process triggers the onset of the second process. Therefore, it is the differential of the first process that should figure under the integral in the first line of Eq. (3), because it is in this converted fraction that the second process will follow.

The curve fitting according to Eq. (3) was performed using the Levenberg-Marquardt algorithm, also known as the damped nonlinear least-squares method. The results of a simultaneous fit of the experimental data of the amorphization and polymerization stages with the Avrami Eq. (2) and double-Avrami Eq. (3) equations, respectively, are shown in Fig. 4 (A, B). The coefficients resulting from the fits are given in Table 1. The fits provide the Avrami parameter of the first stage close to unity, which signifies one-dimensional character of the process. A similar value for the amorphization process may be obtained by applying the Avrami model to the X-ray data from Fig. 2. The Avrami parameter obtained for the second process is close to 0.5 that likely accounts for a diffusion-controlled process. The latter is likely to happen due to the gradual increase of the glass transition temperature, which dramatically slows down the system due to the increase of viscosity. The quality of the fit is satisfactory which shows that the employed model is adequate.

The possibility of the monomer melting as a consequence of the oligomerization reaction is accounted for by the fact that the enthalpy of the chemical reaction is one order of magnitude higher than the enthalpy of melting (i.e. 1050 versus 105 J $g^{-1}$). Fig. 4 (C, D) demonstrates the difference and ratio of the degrees of conversion $\alpha_{am}(t)$ and $\alpha_{pol}(t)$ for the storage of DAPOT at room temperature and at -25 °C. The difference of the conversions pertinent to the stages of the process allows appreciating the fraction of the system which remains in the intermediate state, i.e. after the passage of the amorphization front but before completion of the polymerization (Fig. 5, top). For the annealing process at RT this fraction reaches ca. 20 % after the initial increase and stays at this level for most of the experiment. In contrast, for the annealing at -25 °C the intermediate fraction is larger and more prone to variation, which can be accounted for by a much longer induction time of the polymerization process. The ratio of the two conversions shows the completeness of the chemical transformation of the amorphous fraction. This variable displays a steady increase for the two conditions of storage.

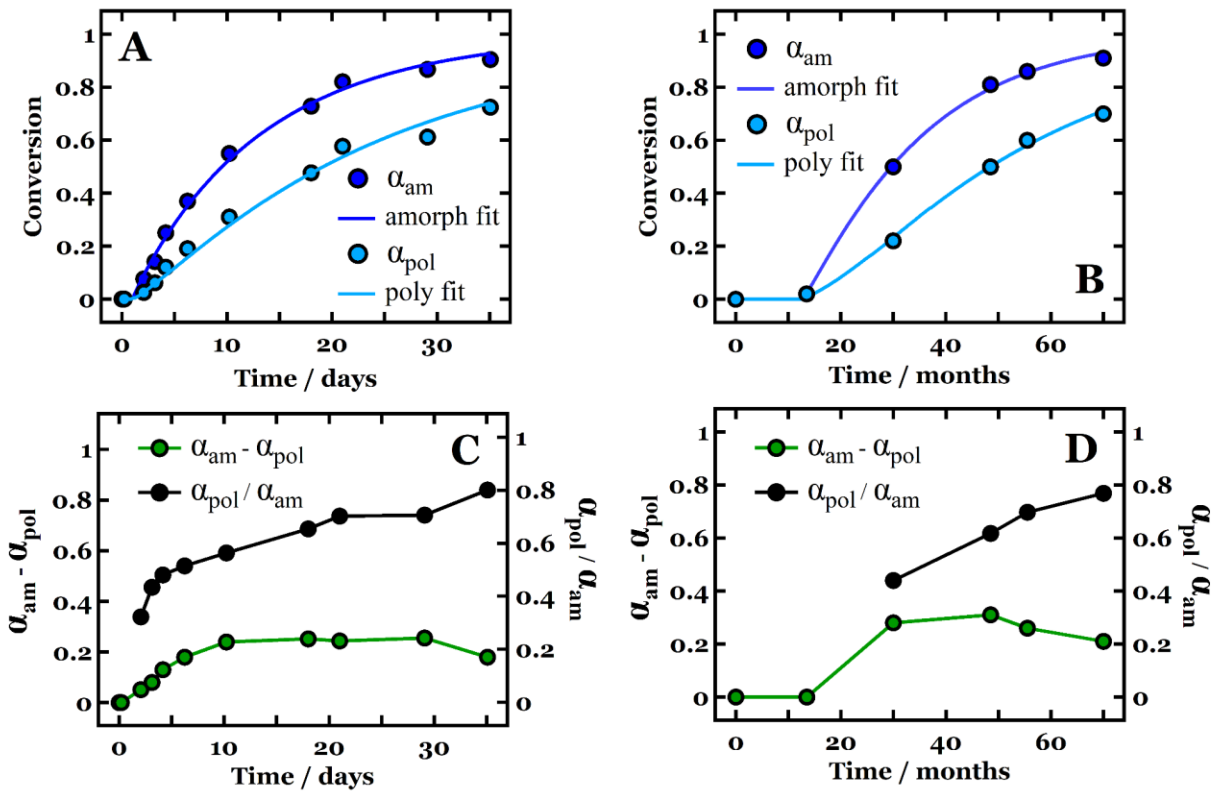


**Fig. 4**. Top row: conversions of the amorphization and polymerization processes for DAPOT calculated from the DSC data at RT (A) and at -25 °C (B). The fits with the double-Avrami model are given in solid lines. Bottom row: difference and ratio between DAPOT degrees of amorphization and polymerization for annealing at RT (C) and -25 °C (D).

**Table 1**. Results of the fits of the DAPOT DSC data.

| Process, conditions | K / time units$^{-n}$ | n | $t_0$ / time units |
|---|---|---|---|
| Amorphization @ RT | 0.088 ± 0.013 days$^{-0.96}$ | 0.96 ± 0.06 | 1.02 ± 0.25 days |
| Polymerization @ RT | 0.276 ± 0.016 days$^{-0.5}$ | 0.50 ± 0.02 | - |
| Amorphization @ -25 °C | 0.031 ± 0.003 months$^{-1.1}$ | 1.10 ± 0.06 | 12.8 ± 0.3 months |
| Polymerization @ -25 °C | 0.121 ± 0.006 months$^{-0.51}$ | 0.51 ± 0.03 | - |

The schematics of the two-stage process is given in Fig. 5. It presents such a consequential transformation as passage of linear fronts of the amorphization and polymerization across needle-like DAPOT crystals. Since the density of the system decreases upon transformation to the amorphous state, the lateral section of the single crystal upon transformation is shown larger accordingly.

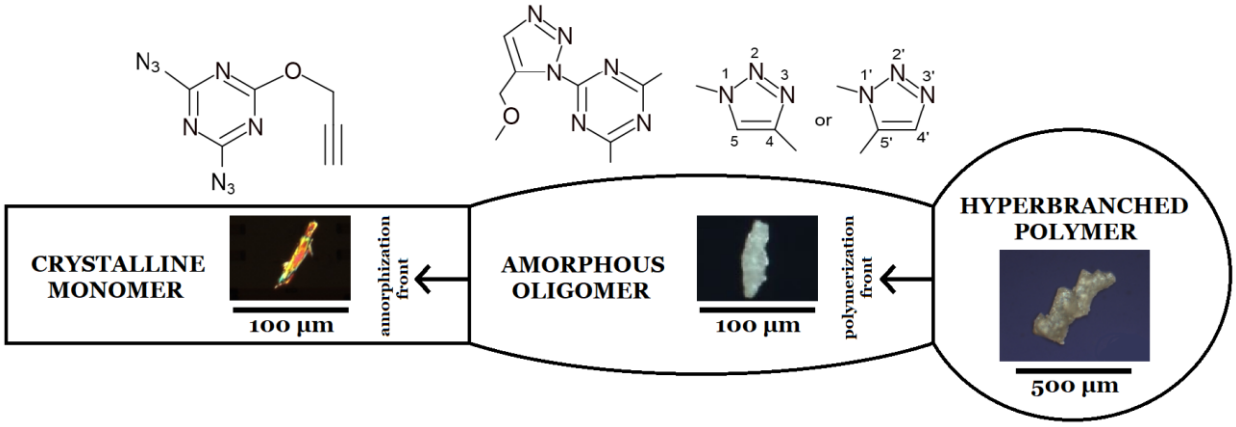


**Fig. 5**. Schematics of a two-stage transformation process of the DAPOT crystalline monomer during long-term storage. The first step represents the oligomerization causing crystal melting, and the second one – the formation of 1,4- or 1,5-disubstituted 1,2,3-triazole products (top row). The micrographs of a fresh monomer microparticle in polarized light (bottom left), partially amorphous oligomerized particle (bottom middle) and a highly amorphous polymerized particle after a year of annealing at 50 °C (bottom right).

Based on the kinetic constants, it is clear that during the long-term storage or slow heating of DAPOT bulk samples they spontaneously undergo oligomerization causing localized crystal melting followed by polymerization. This process results in a change of the sample state and complicates the interpretation of the thermal analysis data. It is therefore instructive to perform a comparative study of the thermal behavior of isolated microparticles during slow and fast heating ramps.

The evolution of crystallinity of microparticles during heating at a very low rate of 1.0 K $min^{-1}$ was studied with polarized optical microscopy by monitoring the shape of particles and intensity of birefringence. Fig. 6 shows the micrographs of the DAPOT monomer particles in a fully crystalline state and the ones that have been stored at -25 °C for two years. One can see that long-term storage results in significant decrease of birefringence. During heating above 50 °C fresh microparticles transform to drops of liquid melt whereas the stored microparticles partially keep their shape that indicates increased viscosity due to topochemical transformation (oligomerization) (Fig. 6 (A, B)). The behavior of ABPOT microparticles is similar but the formation of round melt drops reveals a more limited oligomerization process (Fig. 6 (C, D)).

The integral intensity of birefringence of the DAPOT sample during heating starts to decrease even before the onset of the melting peak (Fig. S2 (B)). Moreover, it can be seen that the peak shifts towards lower temperatures with increasing sample aging time. In contrast, the same time dependence of the intensity of the ABPOT sample does not reveal any visible changes. The increase of the optical density at the melting point can be associated with the effects of light reflection from the interfaces and reorientation of the optical axes of crystals.

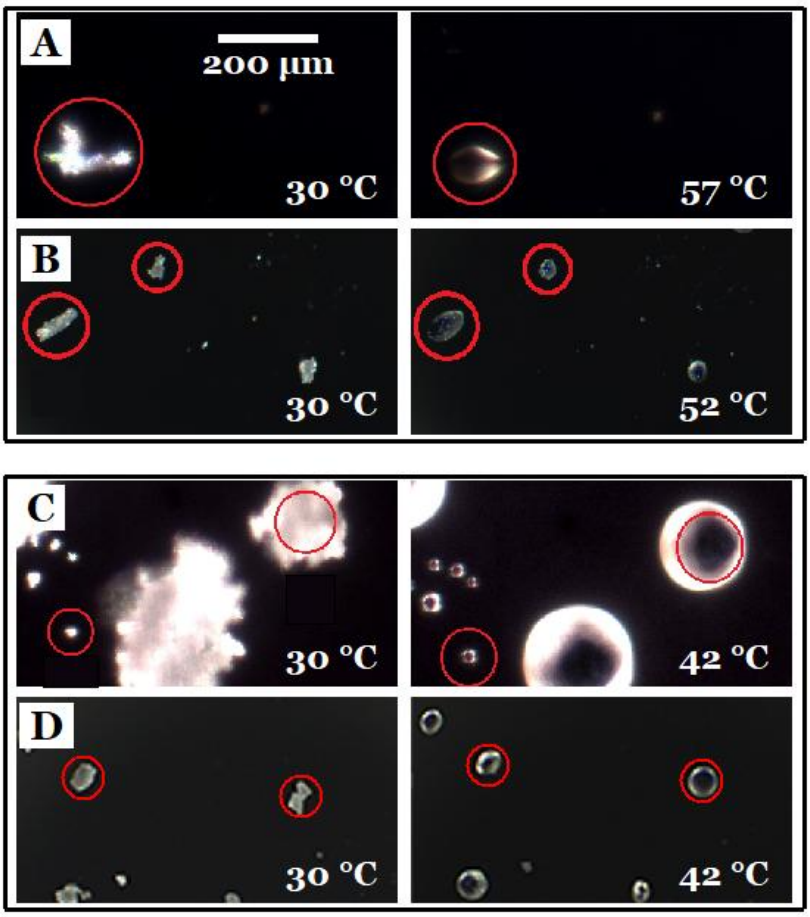


**Fig. 6.** Micrographs of DAPOT (A, B) and ABPOT (C, D) particles during the polarized optical microscopy experiments in the initial state (A, C) and after two years of storage at -25 °C (B, D). The images are recorded at 100X magnification at different temperatures. The colored circles indicate areas of the optical density integration.

It was also expected that the most aged and already polymerized DAPOT microparticles do not reveal melting at all (Fig. S3, black curve). Heating up to 215 °C results in darkening and occasional jumping of the particles due to release of mechanical stresses accumulated during polymerization. Earlier, it was shown that formation of cyclic dimers in monomer volume containing large amounts of azide and alkyne reactive groups can be the reason for the intense energy release due to increase of the mechanical stress during slow heating [37]. Thus, aging of the DAPOT powder leads to the formation of higher molecular weight fractions in microparticles that have thermal properties substantially different from those of the pristine monomer.

This effect of long-term storage on the thermal behavior of microparticles can be visualized during ultrafast heating processes. The FSC curves recorded during heating of both fresh monomers at a heating rate of 1000 K $s^{-1}$ (Fig. 7(A), blue and red curves) exhibit endothermic peaks in the range 55-85 °C corresponding to the monomer melting (Fig. 7(A), region 1). Compared to the DSC data, a small shift of the melting onset can be explained by thermal gradients across the chip active area. At such high heating rates the temperature gradient can sometimes cause offsets of several degrees for microparticles, as described in our previous work [26]. Subsequent broad steps at 200-240 °C reflect a decrease of the sample total heat capacity (Fig. 7(A), region 3, blue, red and purple curves). High-speed camera images show that this step is related to evaporation of low molecular weight fractions (Fig. 7(B) and video from SI). A similar behavior of microparticles during ultrafast heating was found earlier for the case of an RDX explosive [29].

For the studied samples a broad exothermic polymerization peak, observed earlier on the DSC curves (Fig. 1 (A, C) and Fig. 3), is completely absent on the fast heating curves. This proves that FSC experiments allow bypassing the processes with relatively low activation energies by using high heating

rates. Noticeably, the thermal behavior of an aged ABPOT sample coincides with the behavior of the initial monomer, which indicates absence of the oligomeric phase in the microparticle upon fast heating (Fig. 7(A), purple curve).

The FSC curve of an aged DAPOT microparticle also exhibits a weak monomer melting peak (Fig. 7(A), light-blue curve). In contrast to the fresh sample, the effect observed at 130 °C can be assigned to the glass transition of a polymer phase, which is hard to observe in the DSC data because of a rather broad overlapping polymerization peak. At temperatures above 300 °C, one can detect an intense exothermic peak that corresponds to the polymer decomposition accompanied by gas emission and formation of carbonaceous products that cannot be dissolved and removed from nanocalorimetric sensors.

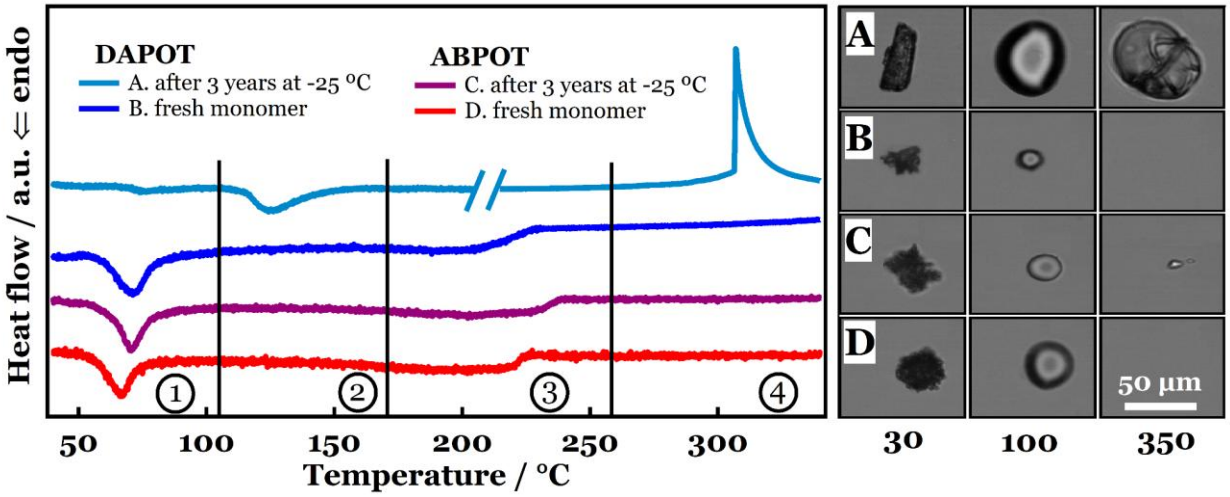


**Fig. 7.** Left (A): nanocalorimetry curves measured at a rate of 1000 K $s^{-1}$ exhibit four regions: (1) monomer fraction melting; (2) polymer fraction glass transition; (3) liquid monomer evaporation; (4) polymer decomposition. The data after the break in the curve are divided by a factor of 10 to demonstrate the intense effect above 300 °C. Right (B): corresponding micrographs of isolated particles with lateral size of about 30-50 microns recorded with an in-situ digital high-speed camera. 30 °C: crystal phase; 100 °C: molten state; 350 °C: after liquid monomer evaporation and/or polymer part decomposition. The curves are shifted vertically for the sake of clarity.

Fully polymerized DAPOT microparticles were obtained when stored at 50 °C, i.e. slightly below the melting point, for a year. Fig. S3 shows comparison of nanocalorimetric heating curves recorded at a rate of 1000 K $s^{-1}$ of DAPOT microparticles in the monomer and polymer states. While a monomeric particle is expected to exhibit melting and evaporation stages on heating, the thermal behavior of a polymerized particle includes only a step in heat capacity associated with its glass transition. The observed shift of the glass transition from 130 to 157 °C for the DAPOT samples stored at 50 and at -25 °C indicates formation of a more developed polymer network for higher temperature storage.

The experiments show that ABPOT is significantly more stable than DAPOT: it does not undergo any visible changes even after 5 years of storage at -25 °C, so it is more challenging to address the thermal behavior and kinetics of its transformations. However, when kept in bulk at temperatures a few degrees below its melting point for a few months a partially amorphous sample can be obtained. Fig. S4 presents comparative data for the original and aged ABPOT samples showing that its thermal behavior is in many respects similar to that of the aged DAPOT samples. The calculated specific enthalpy values of melting (64 J $g^{-1}$) and polymerization (680 J $g^{-1}$) from the DSC data (Fig. S4 (A)) demonstrate that the decrease of crystallinity matches the advancement of the polymerization. Similarly, the nanocalorimetric curve includes an intense exothermic peak at around 300 °C (Fig. S4 (C)) that is assigned to the polymerized particle decomposition which results in formation of black insoluble products (Fig. S5, right).

## 4. Conclusions

Using conventional methods of structural and thermal analysis along with ultrafast chip calorimetry the structural evolution during long-term storage of 2-azido-4,6-bis(prop-2-yn-1-yloxy)-1,3,5-triazine and 2,4-diazido-6-(prop-2-yn-1-yloxy)-1,3,5-triazine monomers was studied.

In contrast to classical topochemical reactions with formation of regular crystalline polymers, the polymerization of the studied monomers yields amorphous products. The transition from crystalline to amorphous state can be observed for DAPOT even during long-term storage at temperatures below 0 °C. This can be explained by the highly exothermic effect of chemical reactions that is about 10 times higher than the melting enthalpy of the monomer crystals. In particular, local thermal fluctuations can activate oligomerization of a monomer leading to a decrease in crystallinity. The interplay between the thermal effect of oligomerization/polymerization and monomer melting has not been previously described in the literature, to our knowledge.

A quantitative kinetic analysis of the amorphization and polymerization processes was carried out by fitting isothermal DSC data with the correlated double-Avrami model. It is shown that the Avrami parameter of amorphization is close to unity while that of polymerization is approx. 0.5. Therefore, both processes can be viewed as one-dimensional, with diffusion-limited mode of polymerization. The latter can probably be explained by the gradual increase of the glass transition temperature, which dramatically slows down the system due to slowing down of segmental dynamics.

With the help of simultaneous optical microscopy and fast calorimetry experiments on isolated microparticles it becomes possible to address their thermal behavior. The thermal experiments on individual microparticles with the help of nanocalorimetry allow bypassing the low activation energy processes of chemical transformation thereby separating them from the thermodynamic transitions such as melting. The results provide additional insights into initial stages of the solid-state polymerization of azide-alkyne monomers on a time scale from milliseconds to years. Such an approach can contribute significantly to optimization of methods of synthesis of hyperbranched polymers, including targeted monitoring of topochemical transformations, as well as their stabilization and determination of storage conditions.

**Supplementary Materials**: Scheme S1. The synthesis scheme of hyperbranched polymers based on monomers ABPOT (a) and DAPOT (b); Fig. S1: TGA curves (10 K $min^{-1}$) of DAPOT (blue) and ABPOT (red) samples obtained in the nitrogen atmosphere during heating from 25 to 900 °C; Fig. S2: Variation of optical density during heating of the ABPOT (A) and DAPOT (B) microparticles. Data obtained by integrating areas with single microparticles from Fig. 6; Fig. S3: Nanocalorimetric curves of DAPOT microparticles of monomer (blue) and polymer (black) samples obtained at a heating rate of 1000 K $s^{-1}$; Fig. S4: Characterization of a partially polymerized ABPOT sample generated by storing it at 30 °C for two months: A — DSC, B — X-ray powder diffraction, C — nanocalorimetry, D — intensity of birefringence measured with polarized optical microscopy; Fig. S5: Micrographs of 3 stages of partially polymerized ABPOT microparticle during a fast-heating nanocalorimetry experiment at a rate of 1000 K $s^{-1}$. Video: Fast heating ramp of a DAPOT microparticle aged for 3 years at -25 °C. Heating rate: 1000 K $s^{-1}$, video recording: 300 fps.

**Author Contributions**: Conceptualization: D.A.I.; Methodology: D.V.A., D.A.I., G.V.M.; Synthesis: A.V.S. and A.O.P.; X-ray analysis: D.A.I., A.V.M. and A.A.P.; Software: A.P.M. and E.V.K.; Supervision: D.V.A. and D.A.I.; Formal analysis: E.V.K.; Investigation: E.V.K. and D.V.A.; Writing: original draft: E.V.K.; Writing—review & editing: D.A.I. All authors have read and agreed to the published version of the manuscript.

**Funding**: This research was funded by Russian Foundation for Basic Research project no. 19-29-12049 and carried out within the framework of the State Assignments (state registration numbers AAA-A19-119032690060-9 and AAAA-A19-119101590029-0).

**Data Availability Statement**: The data presented in this study are available on request from the corresponding authors.

**Conflicts of Interest**: The authors declare no conflict of interest.

**Abbreviations**

The following abbreviations are used in this manuscript:

| | |
|---|---|
| ABPOT | 2-azido-4,6-bis(prop-2-yn-1-yloxy)-1,3,5-triazine |
| DAPOT | 2,4-diazido-6-(prop-2-yn-1-yloxy)-1,3,5-triazine |
| TAAC | topochemical azide-alkyne cycloaddition |
| 1,3-DCA | 1,3-dipolar cycloaddition |
| RT | room temperature |
| WAXS | wide-angle X-ray scattering |
| DSC | differential scanning calorimetry |
| TGA | thermogravimetric analysis |
| NMR | nuclear magnetic resonance spectroscopy |
| FTIR | Fourier transform infrared spectroscopy |
| FSC | fast scanning calorimetry |
| POM | polarized optical microscopy |

**References**


[1] G.V. Malkov, A.V. Shastin, Ya.I. Estrin, E.R. Badamshina, Yu.M. Mikhailov, Synthesis and Characterization of the Nitrogen-Rich Hyperbranched Polymers – Poly([1,2,3]-Triazole-[1,3,5]-Triazine)s, Propellants Explos. 33 (2008) 431–436. https://doi.org/10.1002/prep.200700225

[2] S.N. Vouyiouka, E.K. Karakatsani, C.D. Papaspyrides, Solid-state polymerization. Prog. Polym. Sci. 30 (2005) 10–37. https://doi.org/10.1016/j.progpolymsci.2004.11.001

[3] G. Wegner, Topochemical reactions of monomers with conjugated triple-bonds. IV. Polymerization of bis-(*p*-toluene sulfonate) of 2.4-hexadiin-1.6-diol, Makromol. Chem. 145 (1971) 85–94. https://doi.org/10.1002/macp.1971.021450107

[4] M. Rosenthal, L. Li, J.J. Hernandez, X. Zhu, D.A. Ivanov, M. Möller, A Diacetylene-Containing Wedge-Shaped Compound: Synthesis, Morphology, and Photopolymerization, Eur. J. Chem. 19 (2013) 4300–4307. https://doi.org/10.1002/chem.201203240

[5] A.P. Melissaris, M.H. Litt, High Modulus and High Tg Thermally Stable Polymers from Di-p-ethynylbenzoyl Ester Monomers: Synthesis, Solid State Polymerization; Processing, and Thermal Properties, Macromol. 27 (1994) 2785–2684. https://doi.org/10.1021/ma00088a005

[6] T. Itoh, K. Tachino, N. Akira, T. Uno, M.Kubo, N. Tohnai, M. Miyata, Twofold Helical Polymerization: Thermal Solid-State Polymerization of 7-Cyano-7-(2′-haloethoxycarbonyl)-1,4-benzoquinone Methides, Macromol. 48 (2015) 2935–2947. https://doi.org/10.1021/ma502606s

[7] S. Nomura, T. Itoh, H. Nakasho, T. Uno, M. Kubo, K. Sada, K. Inoue, M. Miyata, Crystal Structures and Topochemical Polymerizations of 7,7,8,8-Tetrakis(alkoxycarbonyl)quinodimethanes. J. Am. Chem. Soc. 126 (2004) 2035–2041. https://doi.org/10.1021/ja0386086

[8] J. Kiji, J. Kaiser, G. Wegner, R.C. Schulz, Solid-state polymerization of derivatives of 2,4,6-octatriyne: 9. Topochemical reactions of monomers with conjugated triple bonds, Polym. J. 14 (1973) 433–439. https://doi.org/10.1016/0032-3861(73)90009-8

[9] G.N. Gerasimov, E.L. Popova, E.V. Nikolaeva, S.N. Chvalun, E.I. Grigoriev, L.I. Trakhtenberg, V.I. Rozenberg, H. Hopf, Ge- and Sn-containing poly(p-xylylene): synthesis, structure and thermal behavior, Macromol Chem Phys, 199 (1998) 2179–2184. https://doi.org/10.1002/(SICI)1521-3935(19981001)199:10%3C2179::AID-MACP2179%3E3.0.CO;2-I

[10] K. Higuchi, K. Sasamura, K. Mizuguchi, Y. Tatewaki, S. Okada, Synthesis and solid-state polymerization of monomers with a conjugated diyne-triene-diyne structure, Polym. J. 54 (2013) 2901–2906. https://doi.org/10.1016/j.polymer.2013.04.018

[11] K. Hema, K.M. Sureshan, Topochemical Azide−Alkyne Cycloaddition Reaction, Acc. Chem. Res. 52 (2019) 3149–3163. https://doi.org/10.1021/acs.accounts.9b00398

[12] G.N. Patel, R.R. Chance, E.A. Turi, Y.P. Khanna, Energetics and Mechanism of the Solid-state Polymerization of Diacetylenes, J. Am. Chem. Soc. 100 (1978) 6644–6649. https://doi.org/10.1021/ja00489a015

[13] X. Meng, H. Chen, S. Xu, Y. Ma, Metal-free 1,3-dipolar cycloaddition polymerization via prearrangement of azide and alkyne in the solid state, CrystEngComm 16 (2014) 9983–9986. https://doi.org/10.1039/C4CE01690D

[14] B.B. Ni, C. Wang, H. Wu, J. Pei, Y. Ma, Copper-free cycloaddition of azide and alkyne in crystalline state facilitated by arene-perfluoroarene interactions, Chem. Commun. 46 (2010) 782–784. https://doi.org/10.1039/B912337G

[15] B.B. Ni, K. Wang, Q. Yan, H. Chen, Y. Ma, B. Zou, Pressure Accelerated 1,3-Dipolar Cycloaddition of Azide and Alkyne Groups in Crystals, Chem. Commun. 49 (2013) 10130–10132. https://doi.org/10.1039/C3CC46153J

[16] G.V. Malkov, A.V. Shastin, Y.I. Estrin, E.R. Badamshina, Yu.M. Mikhailov, New polynitrogen hyperbranched polymers, Russ. Chem. Bull. 60 (2011) 1940–1943. https://doi.org/10.1007/s11172-011-0292-7

[17] M. Rosenthal, D. Doblas, J.J. Hernandez, Ya.I. Odarchenko, M. Burghammer, E. Di Cola, D. Spitzer, A.E. Antipov, L.S. Aldoshin, D.A. Ivanov, High-Resolution Thermal Imaging with a Combination of Nano-Focus X-ray Diffraction and Ultra-Fast Chip Calorimetry, J. Synchrotron Rad. 21 (2014) 223−228. https://doi.org/10.1107/S1600577513024892

[18] A.A. Minakov, S.A. Adamovsky, C. Schick, Non-adiabatic thin-film (chip) nanocalorimetry, Thermochim. Acta. 432 (2005) 177–185. https://doi.org/10.1016/j.tca.2005.01.073

[19] C. Riekel, E. Di Cola, M. Reynolds, M. Burghammer, M. Rosenthal, D. Doblas, D.A. Ivanov, Thermal Transformations of Self-Assembled Gold Glyconanoparticles Probed by Combined Nanocalorimetry and X-ray Nanobeam Scattering, Langmuir 31 (2015) 529−534. https://doi.org/10.1021/la504015e

[20] A.A. Minakov, C. Schick, Ultrafast thermal processing and nanocalorimetry at heating and cooling rates up to 1 MK/s, Rev. Sci. Instrum. 78 (2007) 073902. https://doi.org/10.1063/1.2751411

[21] A.A. Minakov, A. Wurm, C. Schick, Superheating in linear polymers studied by ultrafast nanocalorimetry, Eur Phys J E Soft Matter 23 (2007) 43–53. https://doi.org/10.1140/epje/i2007-10173-8

[22] A.P. Melnikov, M. Rosenthal, A.I. Rodygin, D. Doblas, D.V. Anokhin, M. Burghammer, D.A. Ivanov, Re-exploring the Double-Melting Behavior of Semirigid-Chain Polymers with an in-situ Combination of Synchrotron Nano-Focus X-ray Scattering and Nanocalorimetry, Eur. Polym. J. 81 (2016) 598–606. https://doi.org/10.1016/j.eurpolymj.2015.12.031

[23] M. Rosenthal, A.P. Melnikov, A.A. Rychkov, D. Doblas, D.V. Anokhin, M. Burghammer, D.A. Ivanov, Design of a Combined Setup for Simultaneous Measurements of the Microstructural and Thermo-analytical Parameters of Nanogram-size Samples, Appl. Mech. Mater. 788 (2015) 136–142. https://doi.org/10.4028/www.scientific.net/AMM.788.136

[24] M. Rosenthal, A.P. Melnikov, M. Burghammer, D.A. Ivanov, Reorganization of semicrystalline polymers on heating: Analyzing common misconceptions in the interpretation of calorimetric data. Response on the “Comment on “Re-exploring the double-melting behavior of semirigid-chain polymers with an in-situ combination of synchrotron nanofocus X-ray scattering and nanocalorimetry” by Dimitri A.

Ivanov et al. [Euro. Polym. J. 81 (2016) 598–606.]", Eur. Polym. J. 94 (2017) 517–523. https://doi.org/10.1016/j.eurpolymj.2017.06.036

[25] A.P. Melnikov, M. Rosenthal, D.A. Ivanov, What Thermal Analysis Can Tell Us About Melting of Semicrystalline Polymers: Exploring the General Validity of the Technique, ACS Macro Lett. 7 (2018) 1426–1431. https://doi.org/10.1021/acsmacrolett.8b00754

[26] M. Rosenthal, A.P. Melnikov, A.A. Rychkov, D. Doblas, D.V. Anokhin, M. Burghammer, D.A. Ivanov. Design of an In Situ Setup Combining Nanocalorimetry and Nano- or Micro-Focus X-ray Scattering to Address Fast Structure Formation Processes. In: Schick, C., Mathot, V. (eds) Fast Scanning Calorimetry. Springer, Cham, (2016) 299–326. https://doi.org/10.1007/978-3-319-31329-0_9

[27] M.A. Gorbunova, E.V. Komov, L.Y. Grunin, M.S. Ivanova, A.F. Abukaev, A.M. Imamutdinova, D.A. Ivanov, D.V. Anokhin, The effect of separation of blocks on the crystallization kinetics and phase composition of poly(butylene adipate) in multi-block thermoplastic polyurethanes, Phys. Chem. Chem. Phys. 24 (2022) 902–913. https://doi.org/10.1039/D1CP04684E

[28] E. León-Gutierrez, G. Garcia, A.F. Lopeandia, J. Fraxedas, M.T. Clavaguera-Mora, J. Rodríguez-Viejo, In situ nanocalorimetry of thin glassy organic films, J. Chem. Phys. 129 (2008) 181101. https://doi.org/10.1063/1.3009766

[29] N. Piazzon, M. Rosenthal, A. Bondar, D. Spitzer, D.A. Ivanov, Characterization of explosives traces by the Nanocalorimetry, J Phys Chem Solids 71 (2010) 114–118. https://doi.org/10.1016/j.jpcs.2009.07.032

[30] S.V. Karpov, A.O. Petrov, G.V. Malkov, E.R. Badamshina, The Gaussian G4 enthalpy of formation of propargylamine and propargyloxy derivatives of triazido-s-triazine, Mendeleev Commun. 32 (2022) 338–340. https://doi.org/10.1016/j.mencom.2022.05.015

[31] A.O. Petrov, G.V. Malkov, S.V. Karpov, A.V. Shastin, A.V. Bakeshko, Kinetic Study of the Polyaddition Of Azide-Alkyne AB2 Monomers in Nonisothermic Conditions, Key Eng. Mater. 816 (2019) 151–156. https://doi.org/10.4028/www.scientific.net/KEM.816.151

[32] I.H, Hillier, Modified Avrami Equation for the Bulk Crystallization Kinetics of Spherulitic Polymers, J. Polym. Sci. Part A 3 (1965) 3067–3078. https://doi.org/10.1002/pol.1965.100030902

[33] T. Choupin, B. Fayolle, G. Regnier, C. Paris, J. Cinquin, B. Brule, Isothermal crystallization kinetic modeling of poly(etherketoneketone) (PEKK) copolymer, Polymer 111 (2017) 73–82. https://doi.org/10.1016/j.polymer.2017.01.033

[34] S.A. Chelaghma, O. De Almeida, P. Margueres, J.-C. Passieux, J.-N. Perie, A. Vinet, B. Reine, Identification of Isothermal Crystallization Kinetics of poly(ether-ketone-ketone) based on spherulite growth measurements and enthalpic data, Polymer Crystallization, Wiley 3 (2020) e10141. https://doi.org/10.1002/pcr2.10141

[35] M. Gordon, I. H. Hillier, Mechanism of secondary crystallization of polymethylene, Philosophical Magazine, 11 (1965) 31-41. https://doi.org/10.1080/14786436508211922

[36] B. S. Hsiao, I.Y. Chang, B.B. Sauer, Isothermal crystallization kinetics of poly(ether ketone ketone) and its carbon-fibre-reinforced composites, Polymer 32 (1991) 2799-2805. Hsiao, B. S., Chang, I. Y., & Sauer, B. B. (1991). Isothermal crystallization kinetics of poly(ether ketone ketone) and its carbon-fibre-reinforced composites. Polymer, 32(15), 2799–2805. https://doi.org/10.1016/0032-3861(91)90111-u

[37] A. Ravi, K.M. Sureshan, Tunable Mechanical Response from a Crystal Undergoing Topochemical Dimerization: Instant Explosion at Faster Rate and Chemical Storage of 'Harvestable Explosion' at Slower Rate, Angew. Chem. 57 (2018) 9362–9366. https://doi.org/10.1002/anie.201804589

# SUPPLEMENTARY MATERIAL

# Topochemical polymerization in microparticles of crystalline triazine-based monomers: study by conventional and ultra-fast chip calorimetry

Evgenii V. Komov,[⊥] Alexey P. Melnikov, [⊥, ‡] Alexey A. Piryazev,[⊥,‡] Alina V. Maryasevskaya,[⊥,‡] Artyom O. Petrov, [‡] Georgiy V. Malkov, [‡] Alexey V. Shastin, [‡] Denis V. Anokhin, [*, ⊥, ‡] Dimitri A. Ivanov [*, ⊥, ‡, ‖]

[⊥]Lomonosov Moscow State University (MSU), 1 Leninskie Gory, 119991 Moscow, Russia

[‡]Federal Research Center of Problems of Chemical Physics and Medicinal Chemistry of RAS, Academician Semenov av. 1, 142432 Chernogolovka, Russia

[‖]Institut de Sciences de Matériaux de Mulhouse-IS2M, CNRS UMR 7361, Jean Starcky, 15, F-68057 Mulhouse, France

*Corresponding author: Dimitri A. Ivanov, Email: dimitri.ivanov@uha.fr

The synthesis of ABPOT and DAPOT is described in refs. [1] and [2], respectively. The corresponding structures have been confirmed earlier by elemental analysis (EA), $^1$H NMR, and FTIR spectroscopy: ABPOT: $^1$H NMR, □ (ppm) = 3.66 [t, 2 H, H(7), J=2.4 Hz]; 5.07 [d, 4 H, H(8), J=2.6 Hz]. IR (cm$^{-1}$): 3296 (≡CH); 2143, 1199 ($N_3$); 1555 (triazine); 1327, 1125 ($COCH_2$). Measured (%): C, 47.3; H, 3.1; N, 36.2. $C_9H_6N_6O_2$. Calculated (%): C, 47.0; H, 2.6; N, 36.5. DAPOT: $^1$H NMR, δ (ppm) = 3.69 [d, H, CH, J=2.0 Hz]; 5.08 [d, 2 H, $CH_2O$, J=2.1 Hz]. IR (cm$^{-1}$): 3298 (≡CH); 2140, 1205 ($N_3$); 1580, 1550 (triazine); 1352, 1177 ($COCH_2$). Measured (%): C, 33.4; H, 1.9; N, 57.2. $C_6H_3N_9O$. Calculated (%): C, 33.1; H, 1.4; N, 57.9.

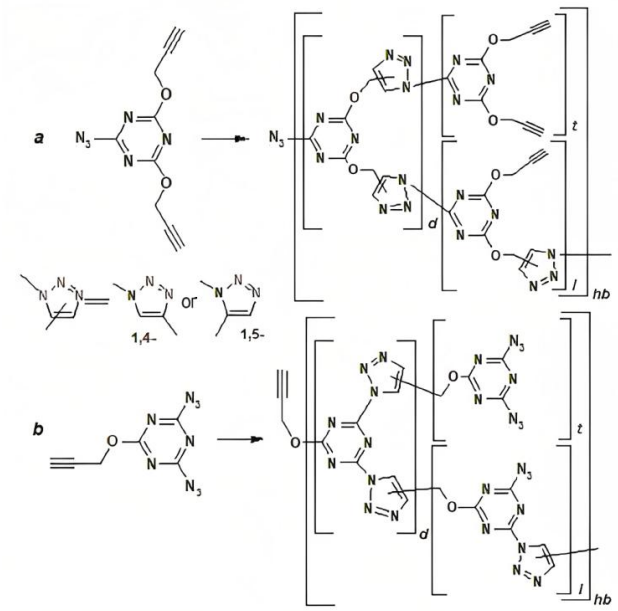


**Scheme S1.** The synthesis scheme of hyperbranched polymers based on monomers ABPOT (a) and DAPOT (b) [3].

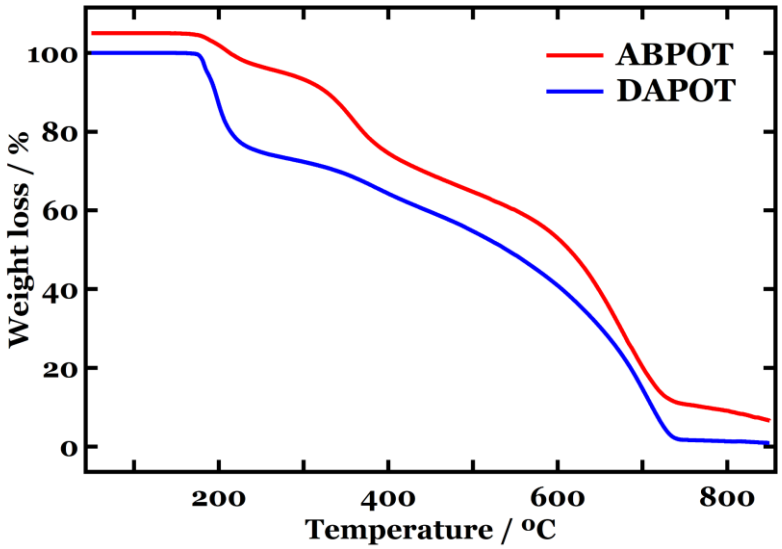


**Fig. S1**. TGA curves (10 K $min^{-1}$) of ABPOT (red) and DAPOT (blue) samples obtained in the nitrogen atmosphere during heating from 25 to 900 °C. The ABPOT curve shifted vertically by 5 % for the sake of clarity.

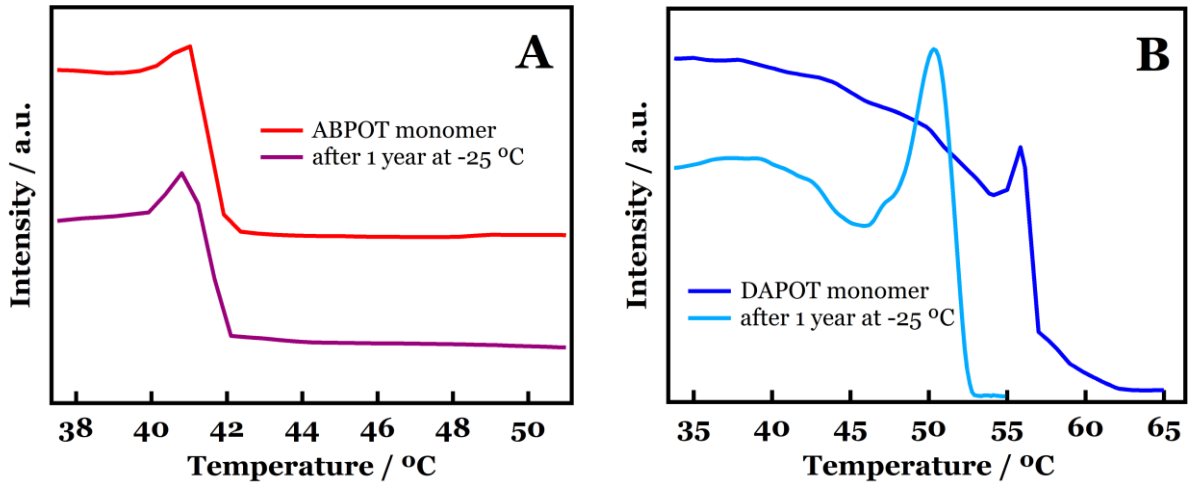


**Fig. S2**. Variation of optical density during heating of the ABPOT (A) and DAPOT (B) microparticles. The data obtained by integrating areas with single microparticles from Fig. 6 of the main text.

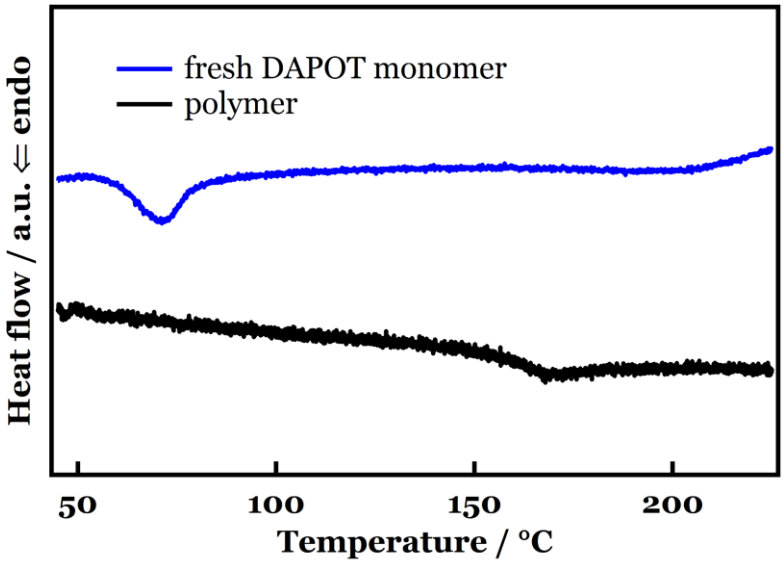


**Fig. S3.** Nanocalorimetric curves of DAPOT microparticles of monomer (blue) and polymer (black) samples obtained at a heating rate of 1000 K $s^{-1}$. The characteristic transitions of the monomer include melting at 57 °C and evaporation above 200 °C. The polymerized particle shows only glass transition at approx. 157 °C.

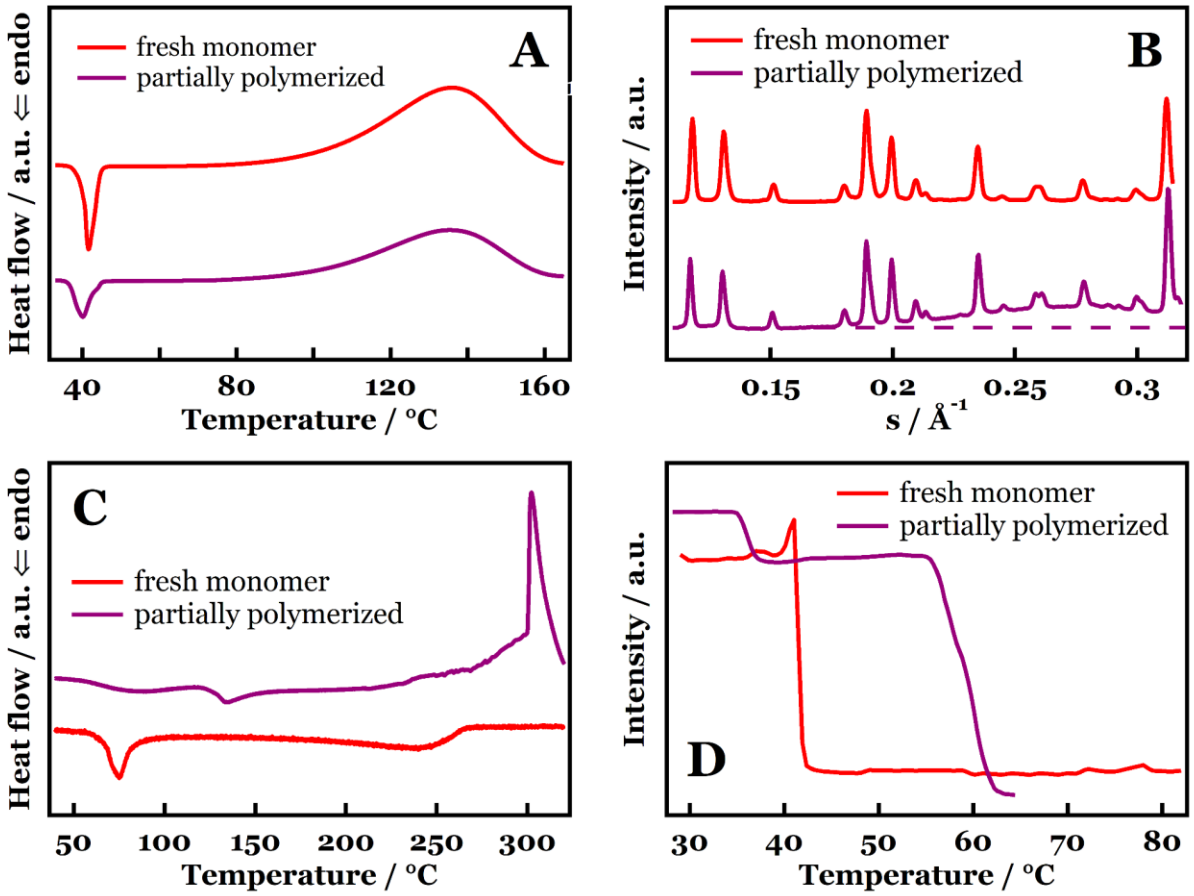

**Fig. S4**. Characterization of a partially polymerized ABPOT sample generated by storing it at 30 °C for two months: A — DSC, B — X-ray powder diffraction, C — nanocalorimetry, D — intensity of birefringence measured with polarized optical microscopy. The curves are shifted vertically for the sake of clarity.

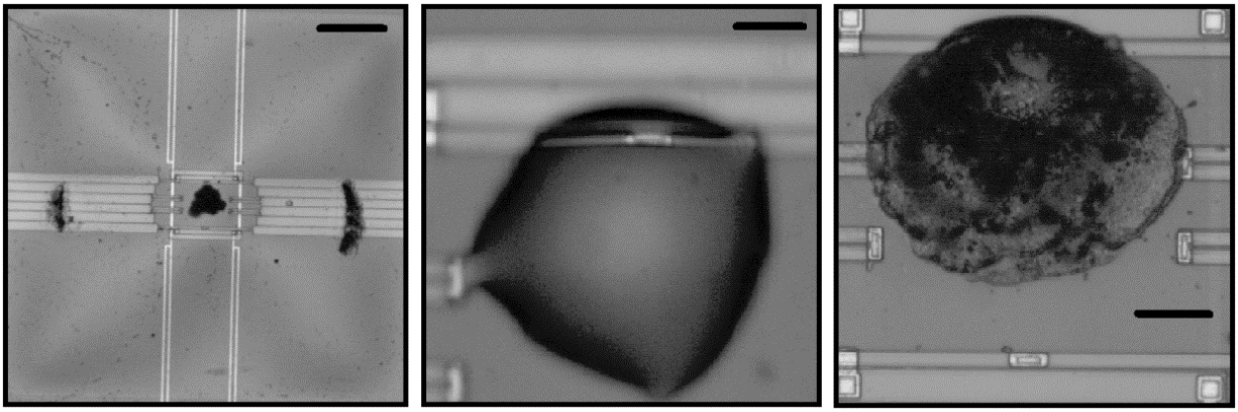

**Fig. S5**. Micrographs of 3 stages of partially polymerized ABPOT microparticle during the fast-heating nanocalorimetry experiment with a rate of 1000 K $s^{-1}$ (cf. Fig. S4, C, purple line) at different temperatures, from left to right: 50, 200 and 350 °C. Scale bars (black horizontal lines) correspond to dimensions of 100, 15 and 20 microns in left, middle and right panels, respectively. Left image shows an initial partially crystalline and partially polymerized microparticle. Middle image shows a mixture of a liquid monomer after melting and an amorphous drop after devitrification. Right image shows carbonaceous products formed after the polymer part decomposition.

**video –** Fast heating ramp of a DAPOT sample aged for 3 years at -25 °C. Heating rate: 1000 K $s^{-1}$, video rate recording: 300 fps.

## References


[1] G.V. Malkov, A.V. Shastin, Ya.I. Estrin, E.R. Badamshina, Yu.M. Mikhailov, Synthesis and Characterization of the Nitrogen-Rich Hyperbranched Polymers – Poly([1,2,3]-Triazole-[1,3,5]-Triazine)s, Propellants Explos. 33 (2008) 431–436. https://doi.org/10.1002/prep.200700225

[2] G.V. Malkov, A.V. Shastin, Y.I. Estrin, E.R. Badamshina, Yu.M. Mikhailov, New polynitrogen hyperbranched polymers, Russ. Chem. Bull. 60 (2011) 1940–1943. https://doi.org/10.1007/s11172-011-0292-7

[3] A.O. Petrov, G.V. Malkov, S.V. Karpov, A.V. Shastin, A.V. Bakeshko, Kinetic Study of the Polyaddition Of Azide-Alkyne AB2 Monomers in Nonisothermic Conditions, Key Eng. Mater. 816 (2019) 151–156. https://doi.org/10.4028/www.scientific.net/KEM.816.151